Reaction Kinetics, Mechanisms and Catalysis (2024) 137:2197–2213
https://doi.org/10.1007/s11144-024-02656-4

Linker-defect assisted catalytic fixation of CO_2 in a dual-linker metal–organic framework

Yunjang Gu[1] · Sunghyun Yoon[1] · Robin Babu[1] · Yongchul G. Chung[1] · Dae-Won Park[1]

Received: 11 March 2024 / Accepted: 13 May 2024 / Published online: 31 May 2024

Abstract

We investigated the effect of linker defects induced by recycling MOF-508, a metal–organic framework with dual linkers, for the catalytic cycloaddition of the CO_2 reaction. MOF-508 catalysts are characterized using various analytical techniques such as powder XRD, FT-IR, FE-SEM, HR-TEM, TGA, BET, NH_3- and CO_2-TPD, NMR, and CO_2 adsorption isotherm. MOF-508 catalysts could perform the coupling reaction between epoxide and CO_2 with > 99% selectivity toward cyclic carbonates under solvent-free and moderate reaction conditions. After the cycloaddition reaction, the recycled MOF-508 exhibited higher catalytic activity than freshly prepared MOF-508 at all the temperature ranges. The origin of increased cyclic catalytic activities was attributed to the creating of additional catalytic active sites from the linker defects. Molecular modeling techniques were used to elucidate the catalytic mechanism and quantify the degree of linker defects in MOF-508.

Yunjang Gu and Sunghyun Yoon have contributed equally to this work.

✉ Dae-Won Park
dwpark@pusan.ac.kr

[1] School of Chemical Engineering, Pusan National University, Busan 46241, Korea

Graphical abstract

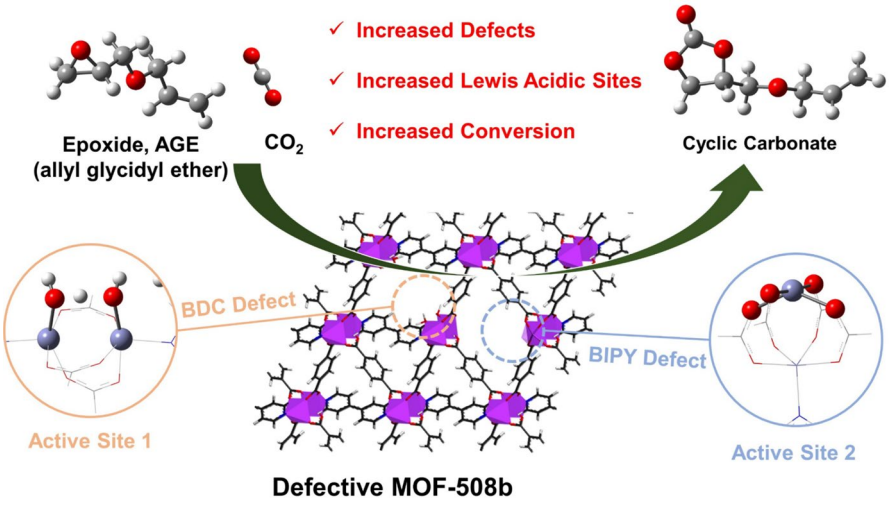

Keywords MOF-508 · CO_2-cycloaddition · Defect · DFT · GCMC

Introduction

Metal–organic frameworks (MOFs) are now well-established porous materials synthesized from secondary building blocks (SBUs) and organic ligands [1–4]. Due to their modular nature, which affords rational tuning of the pore size and high micropore volume, MOFs have been widely investigated for their potential applications in gas storage, separation, and catalysis [5–11]. One such application of MOFs is their utility for catalytic fixation of CO_2 into a five-membered ring, such as propylene carbonate, via cycloaddition reaction [12–21]. The generally accepted mechanism of MOF-catalyzed CO_2 cycloaddition involves the synergistic interplay between the Lewis acid sites of metal centers and the nucleophilic anion of tetraalkylammonium halide co-catalyst, such as tetrabutylammonium bromide (TBAB).

The catalytic active sites in MOFs, such as open metal sites and functional groups, are evenly dispersed throughout the structure and exposed on the crystal surface. Depending on the identity of SBU used in the MOF synthesis, the open metal sites are commonly formed by removing the coordinated residual solvents, defect formation during synthesis, post-synthetic degassing, or post-catalytic recycling steps [22–26]. The degree of MOF defects during synthesis and activation and their impact on the material's performance have been extensively explored [27–31] in the literature. However, less work has been focused on the characterization of framework defects resulting from catalyst recycling and its impact on catalytic performance.

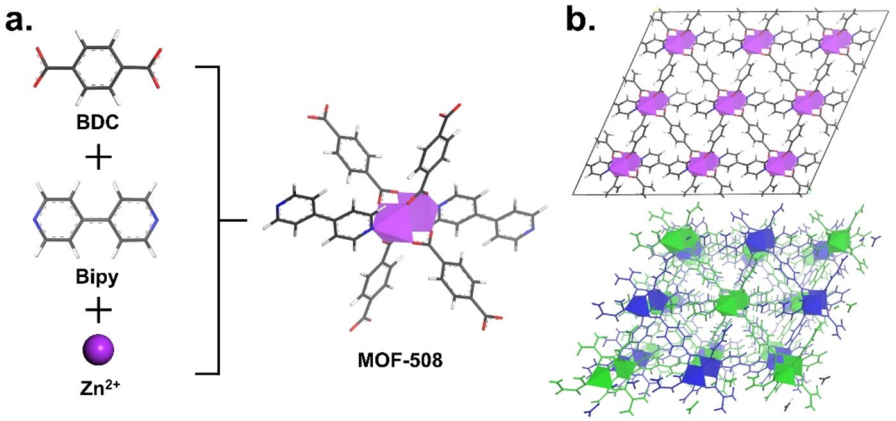

Fig. 1 **a** Schematic representation for the synthesis of MOF-508. **b** 3D porous structure of MOF-508b and twofold interpenetrated structure. Zn, purple; O, red; N, blue; C, gray; H, white. (Color figure online)

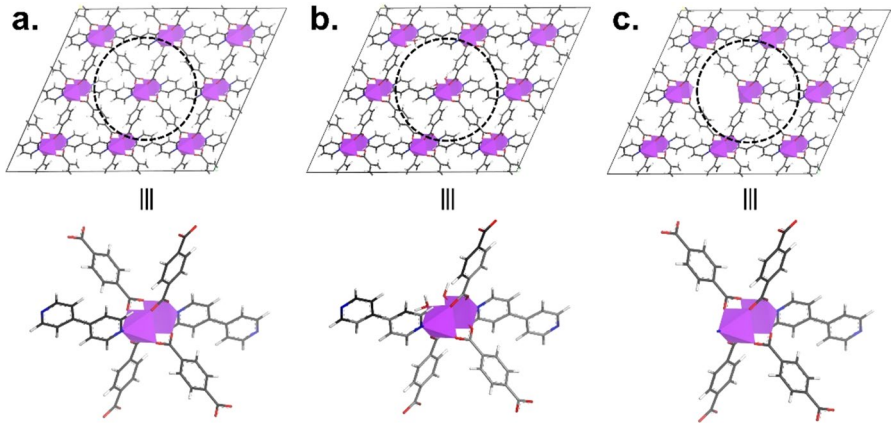

Fig. 2 The pristine and defective structures of MOF-508b. **a** pristine MOF-508b, **b** defective MOF-508b with missing BDC linker, **c** defective MOF-508b with missing 4,4′-Bipy linker

In this work, we prepared one of the dual-linker MOFs, MOF-508 [Zn(BDC)(4,4′-Bipy)] (where BDC = 1,4-benzenedicarboxylic acid, 4,4′-Bipy = 4,4′-bipyridine) [32] as a model catalyst to investigate the CO_2 fixation reaction from framework defects resulting from catalyst recycling. MOF-508 consists of a Zn paddlewheel SBU with two different types of organic ligands (Fig. 1) and has been investigated for the CO_2 cycloaddition reaction [33] at various reaction conditions.

The dual-linker nature allows us to quantitatively characterize types of ligand defects in MOF-508 via the acid digestion method. For example, the removal of 4,4′-Bipy ligand creates open metal sites, while the removal of the BDC ligand creates −OH functional group, which could act as active sites for the cycloaddition of CO_2 and allyl glycidyl ether (AGE) (Fig. 2). Three different MOF samples were prepared

and labeled as MOF-508a (MOF-508 with solvents inside the pore), MOF-508b (F, freshly activated), and MOF-508b (R, 3rd reused). These materials were further characterized using various experimental and simulation characterization tools, such as PXRD, FT-IR, FE-SEM, HR-TEM, density functional theory (DFT), and grand canonical Monte Carlo (GCMC) simulations.

GCMC and the DFT simulations were carried out to quantify the degree of linker defects in MOF-508b and to investigate the reaction mechanisms at the active sites of the catalyst induced by the defects, similar to our previous work [14]. GCMC simulation is a useful tool for estimating the degree of internal defects by comparing N_2 saturation loadings, because the saturation loading increases as the degree of defects increases in the structure. DFT method has been used in the literature to investigate plausible reaction mechanisms for CO_2 cycloaddition reaction at different active sites such as open-metal sites (OMS) [7, 16, 19]. Based on the DFT calculations, the structures and energies of the reaction intermediates and transition states can be determined, which leads to the prediction of the reaction mechanism and activation energy of the reaction pathway.

Experimental

Preparation of catalysts

Synthesis of MOF-508a (guest-filled)

MOF-508a was prepared according to a previous reported method [32]. Typically a mixture of $Zn(NO_3)_2{\cdot}6H_2O$ (0.565 g, 1.9 mmol), terephthalic acid H_2BDC (0.315 g, 1.9 mmol), and 4,4′-bipyridyl (0.147 g, 0.944 mmol) was suspended in DMF/ethanol (1:1, 160 mL), and heated in a 200 mL Teflon lined autoclave at 90 °C for 24 h. The colorless block-shaped crystals formed were collected, washed with DMF and hexane, and dried in air.

Synthesis of MOF-508b (F, fresh, guest-free)

A sample of MOF-508a was heated at 120 °C under a vacuum for 24 h to produce MOF-508b (F).

Characterization of catalysts

Following instrumentations were chosen for the catalyst characterizations: Powder X-ray diffraction (PXRD) patterns were obtained in XPERT-PRO powder diffractometer using Ni-filtered 40 kV CuKα radiation. Fourier transform infrared (FT-IR) spectra were obtained on an Avatar 370 Thermo Nicolet spectrophotometer. The textural properties of the catalysts were analyzed by recording an N_2 isotherm at 77 K with BET instrument (Micromeritics 3-FLEX). Thermogravimetric analysis

(TGA) was performed by raising the temperature from 30 to 800 °C at a heating rate of 3 °C/min under an air flow of 100 mL/min. The surface morphology of samples were analyzed by using SUPRA40VP field emission scanning electron microscope (FE-SEM). The lattice of samples were analyzed by using TALOS F200X high-resolution transmittance electron microscope (HR-TEM) at 200 kV. CO_2 and NH_3-TPD profiles were acquired with a chemisorption analyzer (BET-CAT). Nuclear Magnetic Resonance (NMR) was performed using a Unity-lnova 500 at 500 MHz.

Cycloaddition of CO_2 with allyl glycidyl ether (AGE)

Allyl glycidyl ether (AGE) was selected as a model epoxide in the CO_2-epoxide coupling reaction since it has high boiling point (154 °C) which is useful for high temperature operations. The reactions were performed in a stainless-steel autoclave reactor of 25 mL volume equipped with a magnetic stirrer. The calculated amounts of catalyst, co-catalyst and AGE were charged into the reactor. The coupling reactions were performed for different time intervals using different temperatures and pressures of CO_2. After finishing the reaction time, the reaction mixture was allowed to cool down in an ice-water bath. The final filtrate was centrifuged to remove the catalyst completely and dichloromethane was used as an internal standard for GC analysis using a gas chromatograph (GC, Agilent HP 7890), equipped with a capillary column (HP-5, 30 m × 0.25 mm, flame ionization detector) to determine the conversion, selectivity and yield of the desired cyclic carbonate.

Computational methods

Defect characterization

To model the defective structures for MOF-508b, we constructed missing linker defects in the MOF-508b based on the experimental ^{1}H-NMR analysis. There are two different linkers in the MOF-508b: one is BDC linker and the other is 4,4′-Bipy linker. By removing the two linkers in different numbers, we constructed the defective MOF-508b structures with various relative BDC:4,4′-Bipy ratio. To closely approximate the relative BDC: 4,4′-Bipy ratio (1:0.42) of MOF-508b (R) obtained from the experimental ^{1}H-NMR analysis, the two linkers were removed in various combinations (Table 1). PoreMatMod.jl, one of the open-source Julia package, was used to make missing linker defects in the pristine MOF-508b [34]. If a substructure such as a linker and a main structure such as MOF-508b were specified, the PoreMatModl.jl finds how many the corresponding substructures exist in the main structure and if the number of substructures to be replaced/removed was specified, it removes the substructure or replaces the substructure with another substructure such as another linker. When constructing the missing linker defects in the MOF-508b, we removed 4,4′-Bipy linkers and replaced BDC linkers with formates. Using PoreMatMod.jl, a total of 8 defective structures were constructed with different number of missing linkers.

Table 1 Relative ratio of BDC:Bipy based on the number of missing BDC and 4,4′-Bipy linkers in MOF-508b

		Number of missing 4,4′-Bipy linkers								Model No.
		7	8	9	11	12	13	14	16	
Number of missing BDC linkers	6	**0.42**	0.40	0.38	0.33	0.31	0.29	0.27	0.23	1
	9	0.44	**0.42**	0.40	0.36	0.33	0.31	0.29	0.24	2
	11	0.47	0.44	**0.42**	0.37	0.35	0.33	0.30	0.26	3
	12	0.48	0.45	0.43	0.38	0.36	0.33	0.31	0.26	
	14	0.50	0.48	0.45	0.40	0.38	0.35	0.33	0.28	
	16	0.53	0.50	0.47	**0.42**	0.39	0.37	0.34	0.29	4
	17	0.54	0.51	0.49	0.43	0.41	0.38	0.35	0.30	
	18	0.56	0.53	0.50	0.44	**0.42**	0.39	0.36	0.31	5
	20	0.59	0.56	0.53	0.47	0.44	0.41	0.38	0.32	
	21	0.61	0.58	0.55	0.48	0.45	**0.42**	0.39	0.33	6
	23	0.65	0.61	0.58	0.52	0.48	0.45	**0.42**	0.35	7
	25	0.69	0.66	0.62	0.55	0.52	0.48	0.45	0.38	
	28	0.77	0.73	0.69	0.62	0.58	0.54	0.50	**0.42**	8

The relative ratio of BDC:Bipy is the ratio of the number of remaining 4,4′-Bipy linkers to the number of remaining BDC linkers in MOF-508b. In the pristine MOF-508b, there are 27 4,4′-Bipy linkers and 54 BDC linkers

The values are indicated in bold to highlight the combinations of the number of missing BDC and 4,4′-Bipy linkers in MOF-508b, which has the relative ratio of BDC:Bipy equal to 1:0.42

GCMC simulations were performed to calculate the N_2 saturation loadings (N_2 uptakes at 95,000 Pa) at 77 K for 8 defective structures. The N_2 saturation loading was used to find how many the linkers were removed in the pristine MOF-508b structure. Each GCMC simulation for N_2 saturation loading calculation consisted of 10,000 initialization cycles and 10,000 production cycles for ensemble averages. Translation, rotation, reinsertion, and swap (insertion and deletion) Monte Carlo (MC) moves for N_2 were used for MC sampling with a ratio of 1:1:1:1 (equal probabilities). The Peng-Robinson equation of state was used to calculate the chemical potential from the gas phase pressure and temperature. The Lennard–Jones 12–6 potential was used to model van der Waals interactions between adsorbate–adsorbate and adsorbate-framework. For framework atoms, the Lennard–Jones (LJ) parameters were from the DREIDING force field [35]. The TraPPE force field was used to model N_2 molecule [36]. The Lorentz–Berthelot mixing rules were used to calculate the LJ parameters for different atom type interactions. The interactions were truncated at a cutoff value of 14.0 Å with the analytic tail correction. The periodic boundary conditions (PBC) were applied to all dimensions. Framework atoms were fixed during the simulations. All GCMC simulations were carried out using open-source RASPA 2.0 software [37].

Reaction mechanism

To investigate the mechanism of the cycloaddition reaction between carbon dioxide (CO_2) and AGE catalyzed by MOF-508, the density functional theory calculations have been carried out using the Gaussian 16 Revision A.03 [38] with the B3LYP density functional [39, 40]. The core electrons of Zn atom were modelled with an effective core potential (ECP) with LANL2DZ (Los Alamos National Laboratory 2 Double-Zeta) pseudopotential and C, H, O, N, Br atoms were modelled with the 6–31 + G(d,p) basis set [41–44]. The geometric optimization was followed by vibrational frequency analysis. Minimum energy structures of all the reactants, intermediates (**Int**), and products show no imaginary frequency whereas the transition states (**TS**) are characterized by one imaginary frequency along the bond-breaking/-forming direction. The transition states are confirmed using the intrinsic reaction coordinate (IRC) method. The relative potential energies are provided with respect to the non-interacting systems. The optimized geometries were visualized using GaussView 6 software [45]. Input and output files used in this work can be accessed from: https://github.com/yoonseonghyun/MOF-508.

Due to the large computational cost involved in optimizing the MOF-508 structure, we have constructed two cluster models of the defective MOF-508b. One is a cluster model with an open metal active site formed through a 4,4′-Bipy linker defect, while the other is a cluster model featuring OH^- active site formed by a BDC linker defect. During the geometry optimization, we allowed to relax the active sites and their neighboring atoms, ensuring the fixation of the remaining atoms. In the case of the open metal active site, a single Zn atom and its four nearest O atoms were allowed to relax. For the OH^- active site, relaxation was restricted to OH^-, H_2O, and the two nearest Zn atoms. All other atoms were fixed to maintain the backbone of the original MOF-508b structure.

Results and discussion

The powder X-ray diffraction (PXRD) patterns of the synthesized MOF-508a (Fig. S1), MOF-508b (F), and MOF-508b (R) are compared with simulated MOF-508b (Fig. 3a). The resemblance in the XRD peaks of simulated and synthesized MOF-508b confirms the crystal structure of MOF-508b. However, the MOF-508b (R) showed quite a different XRD pattern from that of the MOF-508b (F), signifying that the structural deformation occurred likely due to the defect formation during the cycloaddition reaction. Chen et al. [32] reported that the X-ray crystal structure of the guest-free phase MOF-508b (DMF removed) reveals that the framework retains the overall connectivity, but the $\{Zn_2(COO)_4\}$ paddle-wheel clusters are significantly distorted, and the 4,4′-Bipy linkers are bent.

Information about the presence of functional groups in the MOF-508b framework was obtained from the FT-IR spectra (Fig. 3b). The broad peak at 3480 cm^{-1} is associated with the stretching vibration of –OH group, while the intense peaks at 1450 and 1070 cm^{-1} can be ascribed to the C=N and C–H stretching vibrations of the imidazole structure, respectively. The FE-SEM image of the MOF-508b shows the

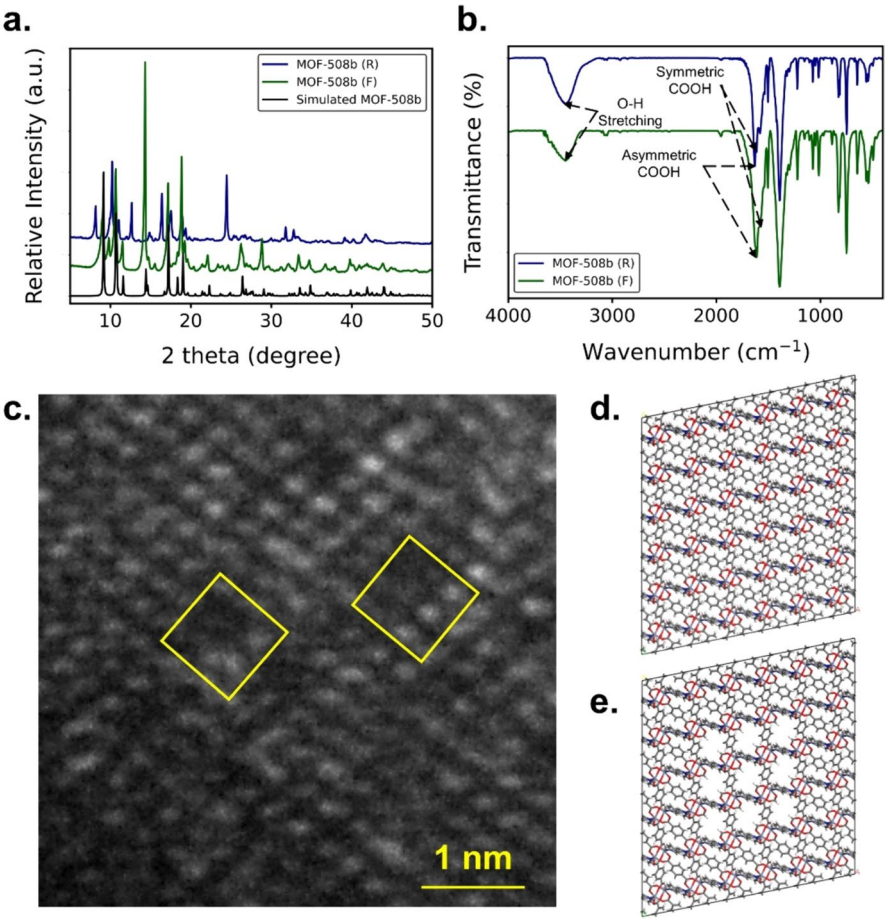

Fig. 3 **a** PXRD patterns of MOF-508b (F) and MOF-508b (R) with simulated MOF-508b. **b** FT-IR spectra of MOF-508b (F) and MOF-508b (R). **c** HR-TEM image of defect in MOF-508b (R), **d** perfect crystal model, and **e** defective structure model

presence of uniformly formed hexahedral-shaped crystals with similar morphology (Fig. S2). XPS analysis (Fig. S3) revealed the presence of Zn. The HR-TEM image of the MOF-508b (R) shows the presence of defects in the lattice structure (Fig. 3c, e).

The number of acidic and basic sites of MOF-508b (F) and MOF-508b (R) were investigated by temperature programmed desorption (TPD) experiments of NH_3 and CO_2, and the TPD results are shown in SI (Fig. S4). Table 2 indicates that higher values of acidity (from NH_3-TPD) and basicity (from CO_2-TPD) are observed for recycled MOF-508b (R) (1.258 and 0.074 mmol/g) than the MOF-508b (F) (0.594 and 0.021 mmol/g). This is likely due to the formation of defects during the cycloaddition reaction, and it will be discussed more in detail at NMR analysis experiments. Furthermore, the thermal behavior and stability of the MOF-508b (F) and

Table 2 Amount of acidic and basic sites in the MOF-508b (F) and MOF-508b (R)

Catalysts	Acidic sites NH_3-TPD (mmol/g)	Basic sites CO_2-TPD (mmol/g)
MOF-508b (F)	0.594	0.021
MOF-508b (R)	1.258	0.074

MOF-508b (R) were verified using TGA analysis (Fig. S5). A weight loss observed at around 100 °C corresponds to the loss of solvent and water in the pore or lattice. A major weight loss was observed after 400 °C, which indicates that the MOF-508b is thermally stable up to approx. 400 °C.

BET analysis was performed to determine the BET area and pore size distributions of the catalyst from the nitrogen adsorption–desorption isotherms at 77 K. The isotherms for MOF-508a, MOF-508b (F), and MOF-508b (R) are presented in Fig. 4a, together with the corresponding their pore-size distribution estimated by 2D-NLDFT method (Fig. 4b). The isotherms of MOF-508a and MOF-508b (F) are very similar containing mostly micropores, except that MOF-508b (F) has higher BET area (724 m^2/g) than MOF-508a (461 m^2/g). This may be originated from the evacuation of solvent molecules in the pores. It was very interesting that MOF-508b (R), recycled after the reaction with AGE and CO_2, showed different adsorption isotherm with hysteresis and the co-presence of larger pores. It signifies the formation of some defects during the cycloaddition reaction by the missing linkers. ^{1}H-NMR study confirmed this defect formation during the reaction, and it will be discussed later. The adsorption capacity of CO_2 at 298 K for MOF-508b (F) and MOF-508b (R) are compared in Fig. S6. The MOF-508b (R) showed higher CO_2 uptake than the MOF-508b (F) catalyst.

Table 3 shows the results of CO_2 cycloaddition with AGE catalyzed with MOF-508b and their precursors at room temperature and 1.2 MPa CO_2 pressure. No significant AGE conversion occurred in 24 h under catalyst-free conditions or in the presence of tetrabutylammonium bromide (TBAB) alone or with the mixture of precursors (Table 3, entries 1–3). MOF-508a exhibited 72% conversion and MOF-508b (F) showed a little higher conversion (76% conversion) than MOF-508a, likely due to increased BET area and pore size. When MOF-508b (F) after the reaction was separated and recycled for the cycloaddition reaction, the MOF-508b (R) showed higher AGE conversion than the MOF-508b (F) catalyst. However, the second and third recycled MOF-508b (R) showed almost equal conversion with the first recycled catalyst (Table 3, entries 6–8). These results suggest a possibility of structural deformation during the cycloaddition reaction. To confirm the superior activity of the MOF-508b (R) catalyst, the cycloaddition reactions were also carried out at high temperatures (80, 100, and 120 °C) with or without the presence of co-catalyst TBAB. As shown in Table 4, all the recycled catalysts still displayed higher AGE conversion than the fresh ones. The MOF-508b (R) catalyst exhibited 96% AGC yield without co-catalyst after 3 h reaction at 120 °C and 1.2 MPa CO_2 pressure. The comparison of MOF-508b with other

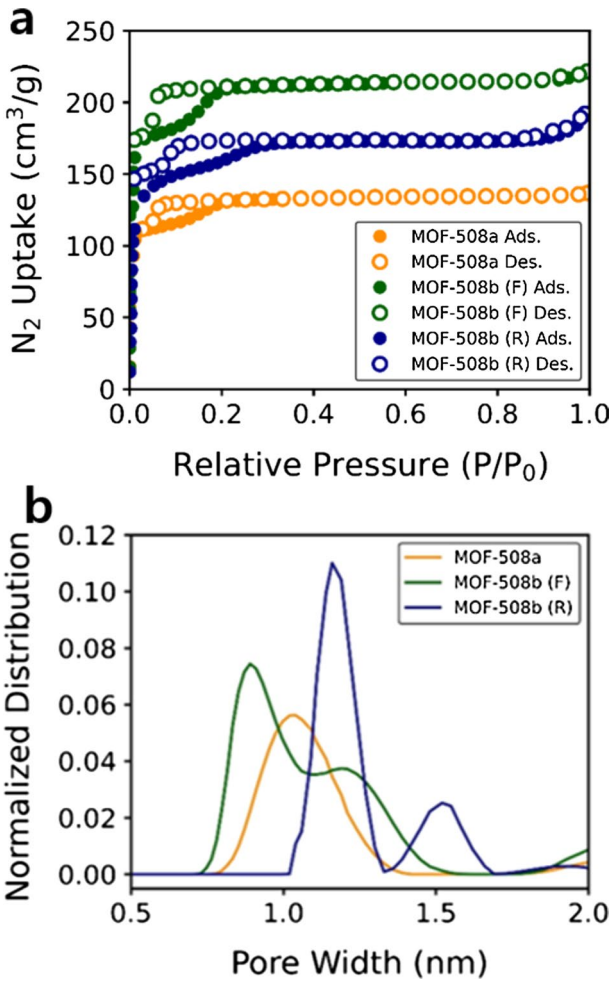

Fig. 4 **a** Experimental N_2 isotherms of MOF-508a, MOF-508b (F), and MOF-508b (R) at 77 K. **b** 2D-NLDFT curves for MOF-508a, MOF-508b (F), and MOF-508b (R). 2D-NLDFT curves were obtained from SAIEUS

previously reported MOFs in Table S1 (in SI) revealed that MOF-508b showed comparable turnover frequency (TOF) in the cycloaddition reaction. Leaching test confirmed that no leaching of Zn metal was observed in the solution after the reaction. To examine the versatility of the MOF-508b, the cycloaddition reactions were performed using various epoxides (Table S2). The terminal epoxides such as propylene oxide, epichlorohydrin, allyl glycidyl ether and the aromatic epoxide, styrene oxide were converted from excellent to moderate rates with the selectivity of over 99%. However, internal epoxide, such as cyclohexene oxide, showed low conversion, likely due to the steric constraint imposed by the bulky functional groups.

Table 3 Cycloaddition reaction of CO_2 with AGE at room temperature

Catalysts	Conversion (%)	Selectivity (%)
None	0	–
TBAB	< 3	–
Zinc + BDC + Bipy	< 10	–
MOF-508a	72	> 99
MOF-508b (F)	76	> 99
MOF-508b (1st R)	80	> 99
MOF-508b (2nd R)	79	> 99
MOF-508b (R)	80	> 99

AGE = 42.8 mmol, Catalyst = 1 mol%, TBAB = 1 mol%, Room temperature, 1.2 MPa CO_2, 24 h, 600 rpm, semi-batch

*(1st R) = 1st reused, (2nd R) = 2nd reused, and (R) = 3rd reused

Table 4 Cycloaddition reaction of CO_2 with AGE at high temperature

Catalysts	TBAB (mol%)	Temperature (°C)	Time (h)	Conversion (%)	Selectivity (%)
MOF-508a	1	80	3	75	> 99
MOF-508b (F)*	1	80	3	82	> 99
MOF-508b (1st R)*	1	80	3	90	> 99
MOF-508b (2nd R)*	1	80	3	90	> 99
MOF-508b (R)	1	80	3	89	> 99
MOF-508a		100	6	60	> 99
MOF-508b (F)*		100	6	67	> 99
MOF-508b (1st R)*		100	6	72	> 99
MOF-508b (2nd R)*		100	6	73	> 99
MOF-508b (R)		100	6	72	> 99
MOF-508a		120	3	85	> 99
MOF-508b (F)*		120	3	90	> 99
MOF-508b (1st R)*		120	3	97	> 99
MOF-508b (2nd R)*		120	3	96	> 99
MOF-508b (R)		120	3	96	> 99

AGE = 42.8 mmol, Catalysts = 1 mol%, 1.2 MPa CO_2, 600 rpm, semi-batch

*(1st R) = 1st reused, (2nd R) = 2nd reused, and (R) = 3rd reused

In order to investigate the defect formation in MOF-508, ^{1}H-NMR study was carried out. 6 mg of dried MOF-508 was digested and dissolved with sonication in 0.6 mL dilute DCl solution (prepared from 50 µL of 35% DCl/D_2O solution (Sigma Aldrich) and 4 mL DMSO-d_6 (Cambridge Isotope Laboratories, Inc.). ^{1}H-NMR data collected on the NMR spectrometer are shown in Figs. S7–S9. The ratio of two linkers BDC:Bipy is summarized in Table 5. From the comparison of the ^{1}H-NMR data of MOF-508a and MOF-508b (F), one can see that the relative composition of the two linker BDC and Bipy was 1:0.38, smaller than the theoretical ratio

Table 5 Ratio of BDC to 4,4′-Bipy of the pristine and defective MOF-508 determined by ^{1}H-NMR

Catalysts	BDC:4,4′-Bipy	Formula from ^{1}H-NMR
MOF-508a	1:0.38	$Zn(BDC)(Bipy)_{0.38}(DMF)_{0.24}(EtOH)_{0.48}$
MOF-508b (F)	1:0.38	$Zn(BDC)(Bipy)_{0.38}$
MOF-508b (R)	1:0.42	$Zn(BDC)(Bipy)_{0.42}$

of BDC:Bipy of 1:0.5, meaning that some defects are present after the preparation step. However, the ratio 1:0.38 remained unchanged even after the evacuation of the solvent DMF and EtOH contained in MOF-508a from its synthesis step. It implies that the structure of MOF-508 was not changed between the two cases. However, after the cycloaddition reaction of AGE and CO_2 with MOF-508b, the relative ratio BDC:Bipy increased from 1:0.38 to 1:0.42, likely due to the defect formation by the missing of some BDC and Bipy linkers, during the cycloaddition reaction. ^{1}H-NMR analysis revealed the possibility of missing linker defects in the MOF-508b (R), which showed higher catalytic activity than the MOF-508b (F).

Molecular modeling was used to quantify the degree of the defects in the MOF-508b. Based on the experimental ^{1}H-NMR analysis, the missing linker defects were constructed in the pristine MOF-508b structure. We constructed different defective MOF-508b structures with various combinations of missing 4,4′-Bipy and BDC linkers (Table 1). Among many defective structures, eight structures were selected where the relative BDC:Bipy ratios correspond to 0.42, which is the ratio of MOF-508b (R). GCMC simulations were performed for the selected eight structures to estimate N_2 saturation loadings (N_2 uptakes at 95,000 Pa) and compared with the N_2 saturation loading of MOF-508b (R). Table 6 shows that the defect model 4, which has 11 missing 4,4′-Bipy linkers and 16 missing BDC linkers, has an N_2 saturation loading value of 7.99 mmol/g closest to the N_2 saturation loading value of MOF-508b (R) of 8.03 mmol/g. Before introducing the linker defects, the pristine MOF-508b had 27 4,4′-Bipy and 54 BDC linkers in the crystalline structure. From

Table 6 Simulated N_2 saturation loadings for 8 defective MOF-508b structures obtained from GCMC results

Model	Number of missing 4,4′-Bipy linkers	Number of missing BDC linkers	N_2 saturation loading (mmol/g)
1	7	6	4.85
2	8	9	5.93
3	9	11	6.44
4	11	16	7.99
5	12	18	8.64
6	13	21	9.71
7	14	23	10.77
8	16	28	12.66

Saturation loadings were N_2 uptakes at 95,000 Pa

this analysis, we could argue that MOF-508b(R) has 41% missing 4,4′-Bipy linker defects and 30% missing BDC linker defects in its crystalline structure.

The generally accepted reaction mechanism for CO_2 and an epoxide to form cyclic carbonate involves three fundamental steps: the epoxide ring-opening, CO_2 insertion, and the carbonate ring-closure [46]. Among these, the epoxide ring-opening step is known to be the rate-limiting step of the reaction. Therefore, we focused on obtaining the transition states for the epoxide ring-opening step and compared the activation energies of the reaction. Initially, the CO_2 addition on AGE is investigated without any catalyst. The energy barrier for the AGE ring opening is found to be 57.8 kcal/mol (Fig. 5a), which is in good agreement with the previous studies (55–63 kcal/mol) [47]. This value suggests that it is essential to use a catalyst to proceed with the reaction.

Previous computational studies show that the Br^- ion from TBAB acts as the nucleophile for the CO_2 cycloaddition reaction. We have employed Br^- with TEA^+ to simulate the large size of the bulky TBAB [48]. Within the defective MOF-508b, two distinct types of active sites are present. The open metal site (OMS), formed by 4,4′-Bipy linker defects, is a well-known catalytic active site for the CO_2 cycloaddition reaction. However, the hydroxyl site (−OH) formed by BDC linker defects is a less explored catalytically active site for the CO_2 cycloaddition reaction in the literature. Here, we used the density functional theory (DFT) calculations to elucidate the catalytic mechanism for the CO_2 cycloaddition reaction for hydroxyl and OMS sites. The relative energies of all the reaction steps for two active sites in the defective MOF-508b are compared in Fig. 5a. As shown in Figs. 5b and S10, for the case of the OMS site in the defective MOF-508b, the reaction is initiated by coordinating AGE on the unsaturated Zn site in the defective MOF-508b to generate an initial coordinated complex $\mathbf{Int_1}$ (− 12.9 kcal/mol). Consequently, bromide ion (Br^-) from the co-catalyst TEAB gets near $\mathbf{Int_1}$ to form a weak van der Waals complex $\mathbf{Int_2}$ with a relative energy of − 22.9 kcal/mol. The Br^- attacks the β-carbon atom of AGE, because of this nucleophilic attack, $\mathbf{Int_2}$ undergoes ring-opening to offer a stable metal-alcoholate species $\mathbf{Int_3}$ via a transition state **TS**. The ring-opening step's activation energy (E_a) is 8.4 kcal/mol. The reaction progresses by the adsorption of CO_2 molecule which forms an intermediate complex ($\mathbf{Int_4}$). After the initial adsorption of the CO_2 molecule, the CO_2 molecule is inserted into Zn–O bond to yield an intermediate complex ($\mathbf{Int_5}$). This intermediate complex ($\mathbf{Int_5}$) is transformed into a new intermediate complex ($\mathbf{Int_6}$) by undergoing intramolecular ring-closing with S_N2 type nucleophilic substitution reaction. After this step, the Br^- nucleophile has been eliminated ($\mathbf{Int_7}$), and the product (AGC) is desorbed, resulting in the regeneration of the MOF-508b catalyst to complete the catalytic cycle of the reaction.

The mechanism on the –OH active site from BDC linker defects in the defective MOF-508b is provided in Figs. 5c and S11. The reaction is initiated by coordinating the oxygen atom of AGE on the −OH group of the defective MOF-508b. Introducing the co-catalyst, Br^- anion, results in an intermediate complex ($\mathbf{Int_2}$) with a relative energy of − 19.0 kcal/mol. The nucleophilic attack of the co-catalyst results in a ring-opening transition state **TS**, and subsequently leads to a new intermediate ($\mathbf{Int_3}$). Here, E_a for ring-opening is 40.6 kcal/mol. The subsequent addition of stable CO_2 molecule results in a new intermediate $\mathbf{Int_4}$ with a relative energy of

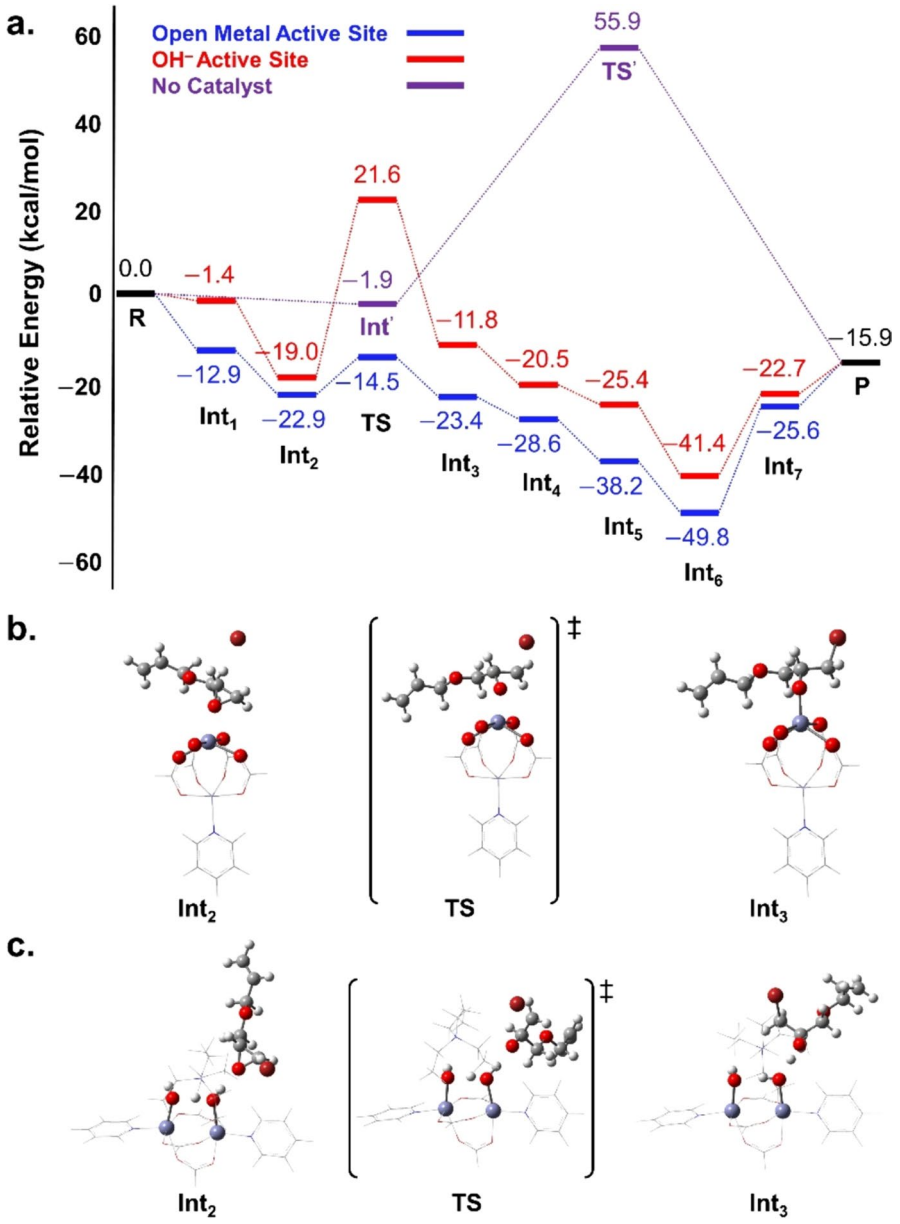

Fig. 5 **a** Relative energy diagram comparison of the cycloaddition reaction of AGE and CO_2 without catalyst (purple) and with the defective MOF-508b/TEAB (the open metal active site resulted from 4,4′-Bipy linker defect (blue) and the -OH active site resulted from BDC linker defect (red)). Optimized geometries of intermediates (**Int$_2$**, **Int$_3$**) and transition state (**TS**) involved in the ring-opening step of the defective MOF-508b/TEAB-catalyzed cycloaddition reaction of AGE and CO_2: **b** Open metal active site and **c** -OH active site. Color code: Zn, slate gray; Br, dark red; O, red; N, blue; C, gray; H, white

− 20.5 kcal/mol. Furthermore, the insertion of the CO_2 molecule results in $\mathbf{Int_5}$ (− 25.4 kcal/mol), which is then transformed into $\mathbf{Int_6}$. Further, AGE and MOF-508b were regenerated.

Our DFT calculations, combined with the NMR data, suggest that the CO_2 cycloaddition reactions occurring at both active sites of the defective MOF-508b exhibit significantly reduced activation barriers (open metal active site: 8.4 kcal/mol, and OH− active site: 40.6 kcal/mol). This reduction may be attributed to the increased Lewis acidic sites resulting from missing linker defects during catalyst recycling. This is consistent with the reports in the literature which show that a high degree of defect leads to improved catalytic performance.

Conclusions

In this work, we synthesized and prepared MOF-508a (guest-filled), MOF-508b (F, guest-free), and MOF-508b (R, 3rd reused after reaction). CO_2 cycloaddition reactions were performed on the catalysts and the materials were characterized by using various physico-chemical techniques. The catalytic activity of these catalysts was examined in the cycloaddition of CO_2 and AGE under solvent-free conditions. The MOF-508b (R) exhibited higher AGE conversion than the MOF-508b (F) and as-synthesized MOF-508a. We found that the recycling of the MOF-508b (F) catalyst leads to a higher conversion of CO_2 cycloaddition reaction. These increased catalytic activities were attributed to MOF-508b (R) possessing a higher amount of acidic and basic sites and mesopores from the cycloaddition reaction-induced framework defects which can favor the activation of epoxide and the mass transfer of reaction mixtures. NMR measurement shows that after the cycloaddition reaction of AGE and CO_2 with MOF-508b, the relative ratio BDC:Bipy increased from 1:0.38 to 1:0.42, likely due to the defect formation by the missing of some BDC linker during the cycloaddition reaction. Molecular simulations were used to quantify the missing 4,4′-Bipy and BDC linkers by comparing the simulated N_2 saturation loadings with the experimental N_2 saturation loading. We found that defect model 4, having 11 missing 4,4′-Bipy linkers and 16 missing BDC linkers, showed N_2 saturation loading close to that of MOF-508b (R). The missing BDC linker creates additional catalytic active sites for the CO_2 cycloaddition reaction. We performed DFT calculations on the –OH site for the plausible CO_2 cycloaddition reaction. We found that the defective MOF-508b reduces the activation energy of the reaction through the −OH active site. On the basis of this, we conclude the improved catalytic performance of defective MOF-508b catalyst could be attributed to the increased Lewis acidic sites and larger pore size of the crystallographic framework resulting from the catalyst recycling.

Supplementary Information The online version contains supplementary material available at https://doi.org/10.1007/s11144-024-02656-4.

Acknowledgements This work was supported by the National Research Foundation of Korea (NRF) grant funded by the Korea government (MSTI) (No. 2020R1C1C1010373). This work was also partially supported by the Industrial Strategic Technology Development Program-Alchemist Project (20012383,

Technical Development of Hydrogen Production from Green Ammonia) funded by the Ministry of Trade, Industry & Energy (MOTIE, Korea). Authors acknowledge the computational time provided by KISTI (KSC-2021-CRE-0066). Authors also acknowledge Soochan Lee (UNIST) for performing NMR measurement on the sample.

Data availability Not applicable.

References

1. Zhou HC, Kitagawa S (2014) Chem Soc Rev 43:5415
2. Furukawa H, Cordova KE, O'keeffe M, Yaghi OM (2013) Science 341:1230444
3. Islamoglu T, Goswami S, Li Z, Howarth AJ, Farha OK, Hupp JT (2017) Acc Chem Res 50:805
4. Li B, Wen HM, Cui Y, Zhou W, Qian G, Chen B (2016) Adv Mater 28:8819
5. Rachuri Y, Parmar B, Bisht KK, Suresh E (2016) Dalton Trans 45:7881
6. Rimoldi M, Howarth AJ, Destefano MR, Lin L, Goswami S, Li P, Hupp JT, Farha OK (2017) Acs Catal 7:997
7. Kurisingal JF, Rachuri Y, Gu Y, Choe Y, Park DW (2019) Inorg Chem Front 6:3613
8. Kreno LE, Leong K, Farha OK, Allendorf M, Duyne RPV, Hupp JT (2012) Chem Rev 112:1105
9. Dhakshinamoorthy A, Heidenreich N, Lenzen D, Stock N (2017) CrystEngComm 19:4187
10. Ahn S, Nauert SL, Buru CT, Rimoldi M, Choi H, Schweitzer NM, Hupp JT, Farha OK, Notestein JM (2018) J Am Chem Soc 140:8535
11. Rahmani E, Rahmani M (2018) Ind Eng Chem Res 57:169
12. Macias EE, Ratnasamy P, Carreon MA (2012) Catal Today 198:215
13. Kim J, Kim SN, Jang HG, Seo G, Ahn WS (2013) Appl Catal A Gen 453:175
14. Gu Y, Anjali BA, Yoon S, Choe Y, Chung YG, Park DW (2022) J Mater Chem A 10:10051
15. Song J, Zhang Z, Hu S, Wu T, Jiang T, Han B (2009) Green Chem 11:1031
16. Babu R, Roshan R, Gim Y, Jang YH, Kurisingal JF, Kim DW, Park DW (2017) J Mater Chem A 5:15961
17. Jeong GS, Kathalikkattil AC, Babu R, Chung YG, Park DW (2018) Chin J Catal 39:63
18. Kim SN, Kim K, Kim HY, Cho HY, Ahn WS (2013) Catal Today 204:85
19. Kurisingal JF, Rachuri Y, Gu Y, Kim GH, Park DW (2019) Appl Catal A Gen 571:1
20. Li Yh, Wang Sl Su, Yc KB, Cy T, Lin Ch (2018) Dalton Trans 47:9474
21. Chen F, Liu N, Dai B (2017) ACS Sustain Chem Eng 5:9065
22. Hall JN, Bollini P (2019) Reac Chem Eng 4:207
23. Kökçam-Demir Ü, Goldman A, Esrafili L, Gharib M, Morsali A, Weingart O, Janiak C (2020) Chem Soc Rev 49:2751
24. Taddei M (2017) Coord Chem Rev 343:1
25. Wu H, Chua YS, Krungleviciute V, Tyagi M, Chen P, Yildirim T, Zhou W (2013) J Am Chem Soc 135:10525
26. Liu L, Chen Z, Wang J, Zhang D, Zhu Y, Ling S, Huang KW, Belmabkhout Y, Adil K, Zhang Y (2019) Nat Chem 11:622
27. Xu Z, Cao J, Chen X, Shi L, Bian Z (2021) Trans Tianjin Univ 27:147
28. Iacomi P, Formalik F, Marreiros J, Shang J, Rogacka J, Mohmeyer A, Behrens P, Ameloot R, Kuchta B, Llewellyn PL (2019) Chem Mater 31:8413
29. Tan K, Pandey H, Wang H, Velasco E, Wang KY, Zhou HC, Li J, Thonhauser T (2021) J Am Chem Soc 143:6328
30. Canivet J, Vandichel M, Farrusseng D (2016) Dalton Trans 45:4090
31. Liu Y, Klet RC, Hupp JT, Farha O (2016) Chem. Commun 52:7806
32. Chen B, Liang C, Yang J, Contreras DS, Clancy YL, Lobkovsky EB, Yaghi OM, Dai S (2006) Angew Chem Int Ed 45:1390
33. Song X, Wu Y, Pan D, Zhang J, Xu S, Gao L, Wei R, Zhang J, Xiao G (2018) Appl Catal A Gen 566:44
34. Henle EA, Gantzler N, Thallapally PK, Fern XZ, Simon CM (2022) J Chem Inf Model 62:423
35. Sl M, Olafson Bd, Wa G (1990) J Phys Chem 94:8897
36. Jj P, Ji S (2001) Aiche J 47:1676

37. Dubbeldam D, Calero S, Ellis DE, Snurr RQ (2016) Mol Simul 42:81
38. Frisch M, Trucks G, Schlegel H, Scuseria G, Robb M, Cheeseman J, Scalmani G, Barone V, Petersson G, Nakatsuji H (2016) Gaussian 16, Revision A. 03, Gaussian. Inc., Wallingford Ct
39. Becke Ad (1988) Phys Rev A 38:3098
40. Lee C, Yang W, Parr RG (1988) Phys Rev B 37:785
41. Pj H, Wr W (1985) J Chem Phys 82:299
42. Wr W, Pj H (1985) J Chem Phys 82:284
43. Clark T, Chandrasekhar J, Spitznagel GW, Schleyer PVR (1983) J Comput Chem 4:294
44. Pc H, Ja P (1973) Theor Chim Acta 28:213
45. Dennington R, Keith TA, Millam JM (2016) Gaussview, Version 6.0. 16. Semichem Inc Shawnee Mission Ks
46. Hu TD, Jiang Y, Ding YH (2019) J Mater Chem A 7:14825
47. Revi P, Mathai G (2016) Chem Sci 5:335
48. Li X, Cheetham AK, Jiang J (2019) Mol Catal 463:37